Preliminary version Modified November 20, 2025

ORIGINAL ARTICLE

Suggestions for unifying the parameterizations that represent turbulent orographic form drag, mountain wave drag and flow blocking

Francois Lott[1*] | **Anton Beljaars**[2*] | **Bruno Deremble**[3†]

[1]Laboratoire de Météorologie Dynamique, Sorbonne-Universite, PSL/Ecole Normale Supérieure,Paris France

[2]European Centre for Medium-Range Weather Forecasts, Reading, UK

[3]Institut des Géosciences de l'Environnement, University Grenoble Alpes, Grenoble, France

Correspondence
Francois Lott, Laboratoire de Météorologie Dynamique, Ecole Normale Supérieure, 24 rue Lhomond, 75231 Paris France
Email: francois.lott@sorbonne-universite.fr

Funding information
VESRI Schmidt Future project DataWave

Parameterizations of subgrid scale mountains are commonly used in numerical weather prediction and climate models. They try to represent quite separate processes namely the enhancement of the turbulent drag by orography, gravity wave drag, and the effects of low level flow blocking. Among the gravity wave schemes, some of them distinguish between upward propagating waves and trapped lee waves. This paper makes use of a recent theoretical methodology to propose a formalism that include all these effects. This theory handles enhanced turbulent drag in the neutral case, gravity waves in the stratified case, and trapped lee waves in the transition. Mountain drag associated to all these processes is estimated analytically, as well as the fraction of the drag that stays within the boundary layer instead of being radiated in the far field. We also try to evaluate the blocked layer depth by combining the sheltering effects that dominate when stratification is small and the blocking effects when stratification is strong.

KEYWORDS
Neutral and stratified boundary layers, orographic turbulent and gravity wave drag, parameterization, trapped lee waves.

[*]Conceptualization, Formal analysis, Methodology, Writing
[*]Formal analysis, Methodology, Writing
[†]Numerical Analysis, Writing

1 | INTRODUCTION

The impact of small to medium scale mountains on the atmospheric dynamics has been intensively studied over the last 50 years by two quite distinct communities. The first community studied how mountains modify the turbulent boundary layer (e.g. Jackson and Hunt, 1975; Beljaars et al., 1987), an issue that is central in the context of wind resource modeling (Ayotte, 2008) or dune formation (Charru et al., 2012). The background theory used neutral and idealized boundary layer closures and analyse how it is modified by small slope orography (Hunt et al., 1988a; Belcher and Hunt, 1998). In this limit, one can consider linear dynamics providing that the problem is formulated using terrain following coordinates. This linear problem is nevertheless still extremely involved and uniform solutions are often obtained via numerical integrations (e.g. Beljaars et al., 1987). These are the basic theories which are adapted to parameterize subgrid scale orography in weather prediction and climate models, initially by increasing the terrain roughness length (Wood and Mason, 1993). Thereafter, Wood et al. (2001) used fully nonlinear simulations to extend the theory and improve the estimate of the depth over which the mountain drag is deposited. This depth estimate is used to formulate a Turbulent Orographic Form Drag (TOFD) parameterization (Beljaars et al., 2004), where the depth over which the drag is deposited becomes related to the horizontal scale of the disturbances. Beljaars et al. (2004) also assumed that the TOFD parameterization should only be used for mountains with horizontal scales $L < 5000$ m. At these scales, and for incident wind U one can expect that the advective time scale, L/U is smaller than the inverse of the Brunt-Vaisala frequency N^{-1}. This ensures that the flow behaves according to neutral flow dynamics.

The second community is more focused on mountain dynamical meteorology. They explain the onset of mountain waves, downslope winds, foehn and trapped waves using theories and models where internal gravity waves control the dynamics, and where the boundary layer is often neglected. The body of theoretical literature on the subject is extremely vast in itself (Durran, 1990). The linear hydrostatic theory yields the development of the earlier orographic gravity wave drag parameterizations (Palmer et al., 1986; McFarlane, 1987), that were used to reduce systematic westerly biases in the upper troposphere. Since then linear theories have also been used to justify the introduction of low level drags due to trapped waves e.g. by Tsiringakis et al. (2017), in this paper to compensate for missing TOFD in the stable case. Prior to that, low level drag was also introduced, because most mountains force large amplitude gravity waves that break at low level (Schär and Durran, 1997) and induce upstream blocking, the flow contouring the obstacle as illustrated by Schär and Smith (1993) in the shallow water case. Although low level wave breaking can be encapsulated in a conventional breaking criteria like in Lindzen (1981), the representation of flow blocking calls for specific diagnostics and drag formulations (Lott and Miller, 1997). All these effects are now taken into account in most weather prediction and climate models (Scinocca and McFarlane, 2000; Kim and Doyle, 2005; Vosper, 2015; Hájková and Šácha, 2024) and their parameterization continue to be improved (van Niekerk and Vosper, 2021). They are often called Subgrid Scale Orography (SSO) parameterizations, which is somehow misleading because TOFD is also a subgrid scale parameterization. According to Beljaars et al. (2004), SSO parameterization should concern mountains with horizontal scale $L > 5000$ m, but remains fully active even in the most recent models which have horizontal resolutions that approach this scale (Sandu et al., 2015; Pithan et al., 2016; Giorgetta et al., 2018). In fact, it is not so clear whether there is a critical mountain size ($L < 5000$ m) below which the mountain would only impact the boundary layer and above which the mountain would only impact the waves. We actually believe that this criterion is quite adhoc and should depend on the nature of the flow. We also know that the effective resolution of a model largely exceeds the gridscale (Vosper et al., 2016), which means that SSO parameterizations will probably remain necessary in the foreseen future and at scales for which TOFD and SSO parameterizations can not be separated.

Because we know that boundary layer dynamics are highly controlled by the inviscid solutions aloft, and because in mountain meteorology the wave forcing is embedded in the boundary layer, it soon appeared that the two com-

munities should make some effort to integrate results from the other community. It is in this context that Hunt et al. (1988a), Belcher and Wood (1996), and Weng et al. (1997) included stratification and gravity waves in boundary layer theories over mountains. Belcher and Wood (1996) showed that when the Froude number $F = U/NL$ is smaller than 1, the mountain drag was due to mountain gravity waves (rather than boundary layer effects) and was well predicted by linear mountain gravity wave theory. This result actually depends on the height at which one chooses the reference velocity U and reference Brunt Vaisala frequency N. A comparable analysis has been made recently in Lott et al. (2023), using a formalism where the gravity wave dynamics is much more complete than in Belcher and Wood (1996), in the sense that it explicitly includes trapped waves and evaluates uniform approximations that can be used to evaluate the vertical profiles of the wave Reynolds stress. As TOFD and SSO parameterizations root in linear theories, and as the neutral results in Lott et al. (2023) reproduce the non-separated sheltering parameterized in TOFD, and the stratified results the trapped and propagating waves parameterized in SSO, it could provide insight on how to combine these two parameterizations.

The main results in Lott et al. (2023) are that the dynamics is controlled by two vertical scales. For an harmonic with horizontal wavenumber k the first is the inner layer scale $h_i(k)$ defined by

$$kU(h_i(k)) \approx \frac{\nu'}{h_i^2}, \tag{1}$$

where $U(z)$ is the background wind profile and ν' the turbulent diffusion coefficient acting on disturbances. The second is the altitude of the turning level height, $h_t(k)$ where the Scorer parameter equals wave number squared:

$$S(h_t) = \frac{N^2}{U^2} - \frac{U_{zz}}{U} = k^2. \tag{2}$$

$h_t(k)$ is the height where upward propagating waves cannot propagate any more and are reflected. The first controls the amplitude of the forcing, the second the nature of the dynamics. More specifically, in the linear case when the mountain height is below and around the inner layer scale, the intensity of the flow that produces inflow disturbances when interacting with the hill is the flow at the inner layer height. For the nature of the dynamics, the flow response is neutral when the turning level is close to the surface compared to the mountain length L, stratified when it is far, and the intermediate situations being associated with trapped lee waves. Although we argue that linear theory could help to combine parametrization of turbulent orographic form drag and subgrid scale orography, the fact that the second includes upstream separation and blocking effects that are not explicitly included in the first, remains a difficulty. To incorporate such effects in the more neutral cases, we need a criterion that can potentially include dowstream separation and sheltering effects. For this purpose, we propose to include non hydrostatic in the blocking criterion, and consider that the linear theory should only take into account the flow above the blocking altitude.

This paper is structured in the following way. Section 2 provides a summary of the theory (Lott et al., 2023), the choices made regarding the background flow properties (unperturbed wind and temperature profiles), and a definition of the relevant dimensionless parameters (Froude number and Richardson number). Section 3 describes results of the linear model classified according to Froude and Richardson numbers, which clearly separates propagating wave, trapped wave and neutral drag regimes. It automatically leads to a physically based scheme for low level drag and how it is distributed in the vertical. Section 3 also discusses briefly how criteria for flow blocking can be extended to included sheltering. Section 4 summarizes and discusses how our results could be used to upgrade state-of-the art TOFD and SSO parameterizations. It also discusses potential remaining issues that remain to be sorted out.

2 | THEORY, BACKGROUND FLOW PROPERTIES, AND DIMENSIONLESS PARAMETERS

Our analysis is based on the linear response to a mountain forcing in the 2D linear Boussinesq equation, using terrain following coordinates X,Z (Lott et al., 2023)

$$x = X, \quad z = Z + h(X) f(Z), \tag{3}$$

where $h(X)$ is the mountain height, and x/z are the horizontal and vertical Cartesian coordinates respectively. Function $f(Z)$ ensures the transition from terrain following coordinates near the surface to Cartesian coordinates by taking $f(0) = 1$ and decaying towards 0 for $Z \to \infty$. The model variables are u (horizontal wind), w (vertical velocity), $\mathbf{w} = u\frac{\partial Z}{\partial x} + w\frac{\partial Z}{\partial z}$ (velocity perpendicular to Z =cte surfaces), p (pressure), and b (buoyancy, defined as $g\theta/\theta_r$ with g for gravity, θ for potential temperature and θ_r a constant reference value). Model variables are expanded in a background in capitals and perturbations primed i.e. $u = U + u'$, $p = P + p'$ and $b = B + b'$. w and $\mathbf{w}$ are perturbations only, i.e, $w = w'$ and $\mathbf{w} = \mathbf{w}$'.

Following Clark (1977) and assuming small perturbations, a set of linear stationary Boussinesq equations can be derived. They contain a turbulent viscosity and given the linearity they can be most conveniently solved in wave number space (see Lott et al., 2023, for details and the Appendix for the equations). For simplicity, mixing length closure is used without considering stability effects in a standard boundary layer approximation which neglects horizontal turbulent fluxes. The vertical fluxes of momentum and buoyancy are

$$\tau = \nu \frac{\partial u}{\partial Z}; \text{ and } q = \nu \frac{\partial b}{\partial Z} \text{ with } \nu = l^2 \left\| \frac{\partial u}{\partial Z} \right\|, \tag{4}$$

where l is the mixing length and $\kappa = 0.4$ the Von Karman constant. To simplify the theory in the outer layer Lott et al. (2023) take

$$l = l_\infty \tanh\left(\kappa \frac{Z + z_0}{l_\infty}\right), \tag{5}$$

rather than the Blackadar (1962) expression valid for neutral flows. It keeps $l \approx \kappa Z$ near the surface and $l \approx l_\infty$ in the far field but avoids a significant log-dependence of the background winds in the far field. With this expression, the horizontal wind and buoyancy profiles that give uniform fluxes are

$$U_V(Z) = \frac{u_*}{\kappa} \log\left(\frac{\sinh \kappa (Z + z_0)/l_\infty}{\sinh \kappa z_0/l_\infty}\right), \; B_V(Z) = \frac{b_*}{\kappa} \log\left(\frac{\sinh \kappa (Z + z_0)/l_\infty}{\sinh \kappa z_0/l_\infty}\right), \tag{6}$$

u_* and b_* being the friction velocity and buoyancy scale respectively. The Brunt-Vaisala frequency is given by,

$$N^2(Z) = \frac{dB_v}{dz} = \frac{b_*}{l_\infty} \left[\tanh\left(\kappa (Z + z_0)/l_\infty\right)\right]^{-1}. \tag{7}$$

As in (6) $U_V(\infty) = \infty$, gravity waves can not propagate in the far field. Therefore, the background velocity is modified to become

$$U(Z) = \frac{u_* d}{l_\infty} \tanh\left[\frac{l_\infty}{u_* d} U_V(Z)\right]. \tag{8}$$

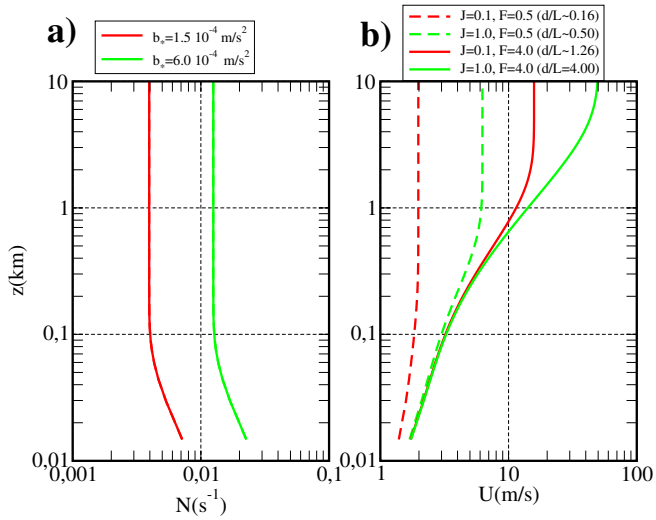

FIGURE 1 Background profiles of Brunt-Vaisala frequency (left panel) and wind (right panel) for two turbulent buoyancy scales b_* and two Froude numbers F. All the other parameters are fixed: $u_* = 0.25$m/s, $l_\infty = 20$m, $z_o = 1$m, and $L = 1$km. Boundary layer depth d is controlled by eq. 10.

which introduces a boundary layer depth d above which the background flow is externally imposed rather than being an exact solution of the viscous equations.

In Lott et al. (2023) disturbance equations are solved for Gaussian mountains

$$h(x) = He^{-\frac{x^2}{2L^2}}, \tag{9}$$

with H and L the mountain height and horizontal length respectively. The far field profile characteristics and the horizontal mountain scale define a Froude number F which turns out to be highly relevant for the flow regime as will be shown later.

$$F = \frac{U(\infty)}{N(\infty)L} = \frac{d}{L\sqrt{J}}. \tag{10}$$

Here J is a Richardson number measured in the boundary layer above the surface layer

$$J = \frac{l_\infty b_*}{u_*^2} \approx \frac{N^2}{U_z^2} (l_\infty << z << d). \tag{11}$$

For fixed F, it will be used to distinguish "neutral" and "stratified situations".

Examples of vertical profiles of $N(Z)$ and $U(Z)$ according to Eqs. (7) and (8) are shown in Figs. 1a and 1b respectively. In them, we choose quite strong values for the friction velocity, roughness length, and limit value of the mixing length which explicitly assumes that we consider rough terrain. The Brunt Vaisala frequency in Fig. 1 decreases uniformly with altitude, as expected when colder surfaces impose stratification but stays quite small when $b_* = 1.5\,10^{-4}$ m/s^2 (red in Fig. 1a). In this case, its minimal value in the far field is $N(\infty) \approx 3\,10^{-3}$ s^{-1} which we will consider as almost neutral flow. For larger b_*, (green in Fig. 1a) the Brunt Vaisala frequency $N(\infty) \approx 1.253\,10^{-2}$ s^{-1},

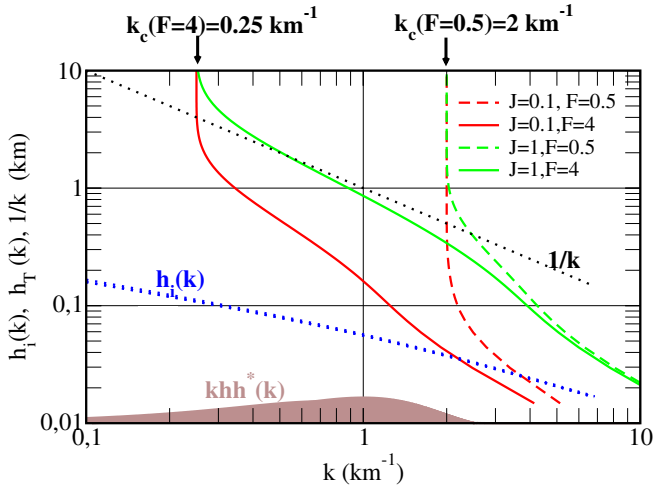

FIGURE 2 Mountain power spectrum multiplied by k for the Gaussian hill with L=1km (brown) and turning levels (red and green) as a function of horizontal wavenumber for the same parameters as in Fig. 1. The dotted curves are the inner layer depth $h_i(k)$ (blue) and $1/k$ (black).

which is quite common for the free atmosphere in a stable winter configuration. The background wind in Fig 1b is shown for the same values of the turbulent buoyancy scale with two different values of the Froude number. In this paper we make the choice to keep the boundary layer characteristics constant (except to distinguish neutral and stratified situations according to b_*). The horizontal scale of the mountain L is set to 1km. These choices make depth d dependent on the Froude number F and b_* (or J) (see eq. 10). For neutral configurations and small Froude numbers, this results in a d that is quite small, the boundary layer stays confined near the surface, and the background wind is small at all altitudes with typically $U < 2$m/s. We will present results for this case for completeness but will mostly detail the other configurations which look more reasonable. In them the incident wind varies from moderately strong in the far field to very strong when d/L changes from $d/L = 0.5$ to $d/L = 4$.

When slope $S = H/L << 1$ and the limit value of the mixing length $l_\infty << L$, Lott et al. (2023) search disturbances to the background winds in the form of Fourier transforms:

$$w'(X,Z) = \int_{-\infty}^{+\infty} \widehat{w}(k,Z) e^{ikX} dk \,. \tag{12}$$

with similar expression for b', p', u', and $\mathbf{w}'$, the disturbances of buoyancy, pressure, horizontal velocity, and velocity perpendicular to the $Z = cte$ surfaces respectively. The disturbance equations considered in Lott et al. (2023) are written in dimensional form in the Appendix, they are solved using matched asymptotics which permits to impose no-slip boundary conditions in $Z = 0$ ($\widehat{u} = \widehat{w} = \widehat{b} = 0$) and radiation condition in $Z \to \infty$, i.e.

$$\widehat{w}(k, Z \approx \infty) = A(k) e^{i\sqrt{(k_c^2 - k^2)}\, Z}, \tag{13}$$

where the "cut-off" wavenumber $k_c = 1/(FL)$ and $k > 0$ to ensure upward propagation and with the convention $\sqrt{-1} = i$ to ensure evanescent waves when there are turning levels (when $k > k_c = 1/(FL)$). The solution for $k < 0$ is obtained by complex conjugation and the amplitude of each harmonics $A(k)$ deduced from the surface boundary

conditions after integration of (31).

To anticipate the response to the mountain forcing, Fig. 2 shows the mountain forcing $\widehat{h}(k)$ in spectral space, the turning levels, and the inner levels as a function of horizontal wavenumber. The altitudes of the inner levels are visualized by displaying $\sqrt{Q(z)}$ on the k-axis, and the turning levels by inverting numerically eq. (1) using for ν' the diffusion coefficient in eq. (31),

$$k\,U(h_i(k)) = \frac{2\,I\,u_*}{h_i(k)^2}. \tag{14}$$

The first thing to notice is that the inner levels depend little on the J and F parameters. There are four almost undistinguishable blue dotted curves, and they are always located at substantially lower altitude than the turning levels. It means that in all cases and for most harmonics there is a large space between the inner layer and the turning levels where the dynamics is predominantly inviscid. The second thing to notice is that for small Froude number ($Fr = 0.5$, dashed lines) most of the harmonics forced by the mountain are not trapped, i.e. $k < k_c$ for most k where the power spectrum of h is large. This is in contrast with the cases at larger Froude number ($F = 4$, solid lines) where most of the harmonics are trapped, i.e. $k > k_c$ for most harmonics forced by h. Still for the larger F, if we contrast cases between neutral and stratified, one sees that more of the trapped waves have turning levels located nearer the surface in the neutral case (solid red line) than in the stratified case (solid green line). According to Lott et al. (2023) this potentially favours the development of trapped lee-waves provided that the turning level altitudes are larger or comparable to the horizontal scale of the disturbances. To substantiate the comparison harmonic by harmonic, the black dotted curve shows their horizontal scale $1/k$. In the stable case ($J = 1$ in solid green), $h_t(k) \approx 1/k$ and becomes even larger when $k < 0.4\,\mathrm{km}^{-1}$. The turning levels are now sufficiently elevated compared to the horizontal scales for trapped waves to develop. On the contrary, in the neutral case ($J = 0.1$, solid red) , $h_t(k) << 1/k$, except of course when the harmonics are no longer trapped (i.e. when $k > k_c$).

3 | LINEAR RESULTS

3.1 | Vertical velocity field

We plot in Fig. 3 the vertical velocity field w' when the outer flow has parameters as in Fig. 1. The first interesting thing to notice is that in all panels, w' has characteristic amplitudes around 50 cm/s which scale as $U(h_i)H/L$, provided we take the velocity at characteristic height $h_i \approx 100\,\mathrm{m}$ (see Fig. 2) and $U(h_i) \approx 2\,\mathrm{m/s}$ (see Fig. 1a). This is the amplitude of the vertical velocity produced when an inviscid flow of speed $U(h_i)$ passes over a ridge of slope H/L. The interpretation given by Lott et al. (2023) is that below h_i dissipative effects force streamlines to be displaced in the vertical following the mountain, and above that inviscid dynamics takes over. This result will be central in our estimations of the drag and stresses. If we now analyse the differences, we see that for small Froude number (Figs. 3a-c) the response is dominated by upward propagating waves with almost no trapped waves in the neutral case (Fig. 3a) and quite a weak low level signal in the stratified case. Note nevertheless that at low level, the vertical velocity presents oscillations with wavelength $\lambda = 2\pi/k \approx 3km$ which is near the "cut-off" wavelength $2\pi/k_c$. This predominance of trapped oscillations near the cut-off wavelength is discussed in detail by Pauget et al. (2024). The results at larger Froude number in Fig. 3b and 3d show much less upward propagating waves, consistent with the fact that most harmonics encounter turning levels. There is nevertheless a strong contrast between the neutral and stratified configuration: trapped modes are almost absent in the neutral case, whereas a quasi-resonant mode dominates in the stratified case. Its horizontal wavelength is around $2\pi/\lambda \approx 15\,\mathrm{km}$, which is significantly smaller than the "cutoff

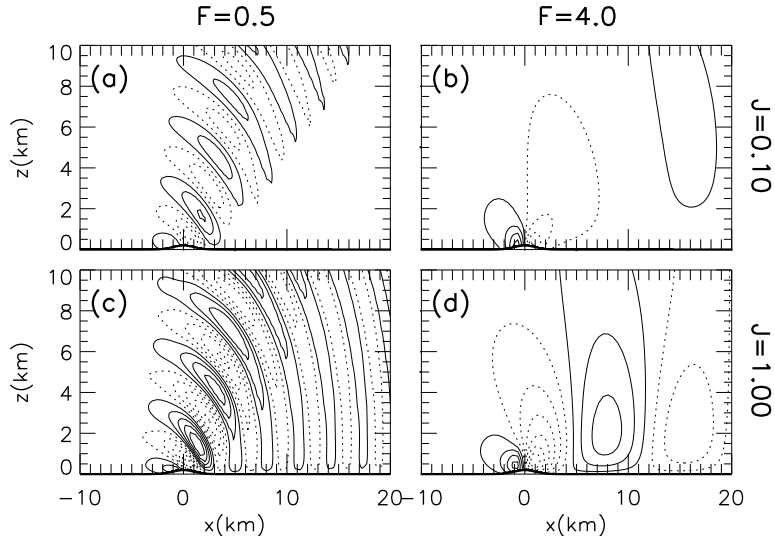

FIGURE 3 Vertical velocity field for various values of J and F, in all simulations $u_* = 0.25\,\mathrm{m/s}^{-1}$, $\lambda = 20\,\mathrm{m}$, z_0=1 m, $L = 1\,\mathrm{km}$, and the mountain height $H = 200\,\mathrm{m}$. To keep F unchanged when J varies, the boundary layer depth $d = \sqrt{J}FL$. In all panels, the contour interval is 10 cm/s.

wavelength" $2\pi/k_c \approx 25\,\mathrm{km}$, a behaviour also discussed in detail by Pauget et al. (2024). Basically, when stratification increases the turning level altitude, the higher turning levels approach the cut-off frequency. When they are sufficiently high compared to the characteristic scale of the mountain, trapped modes start to propagate downstream. It occurs first near the cut-off wavelength, eventually moving to higher wavelengths when the turning levels become higher.

3.2 | Pressure drag and wave Reynolds stress

To estimate the contribution of each harmonic to drag and stress, we compute the momentum flux in terrain following coordinates along Z = cte surfaces

$$\widehat{D}(k,Z) = \Re\left\{-\rho_r \widehat{u}\widehat{\mathbf{w}}^* + ikf(Z)\hat{h}\widehat{p}^*\right\}. \tag{15}$$

The star indicates complex conjugate, $\Re$ is the real part and the function $f(Z)$ is from the curved coordinate definition (3). At $Z = 0$ for instance $f(0) = 1$ and (15) is the mountain drag since $\widehat{\mathbf{w}} = 0$ whereas for $z \to \infty$, the Z-surfaces are horizontal, $f(Z) = 0$, and the formula gives the conventional Reynolds stress since $\widehat{\mathbf{w}} = \widehat{w}$. Note that formula (15) is the representation in spectral space of the leading order of equation (32) in Lott et al. (2023).[1]

The black and red solid lines in Figs. 4 show the contributions of each harmonic to the surface drag and to the gravity wave stress in the far field, $\widehat{D}(k,0)$ and $\widehat{D}(k,\infty)$, respectively. When the Froude number is small in Figs. 4a and 4c, one sees that the Reynolds stress and mountain drag almost coincide. They are both substantial when the harmonics propagate upward in the farfield (when $k < k_c$), they are both small where the harmonics are evanescent

[1]The total drag will need a 2π: $D = 2\pi \int_{-\infty}^{+\infty} \mathbf{D}dk$

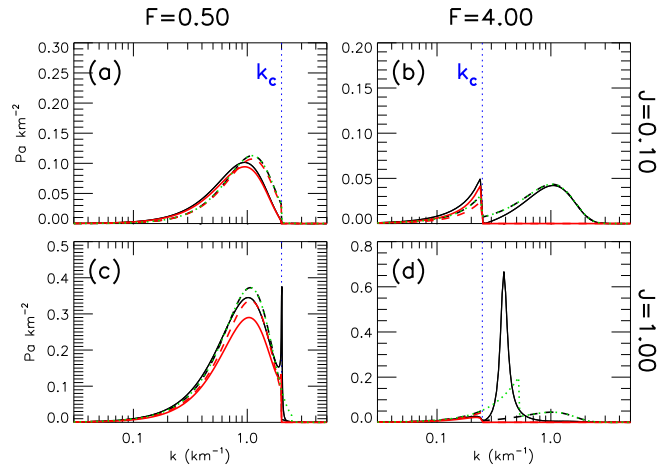

FIGURE 4 Surface drag (black solid line) and wave Reynolds stress (red solid line) as a function of horizontal wave number. The curves represent $k\widehat{D}$ rather than $\widehat{D}$, expressed in Pa/km^{-2} to preserve integration along the log-scale used for the k-axis. The dashed red curve is for gravity wave predictor eq. (16) with $C_W = 0.4$ and the black dashed curve also includes the form drag predictor according to eq. (18) with $C_T = 0.1$. Additionally, the green dotted line includes evanescent modes according to eq. (19) with $S_t = 1$.

in the farfield. Nevertheless when $k < k_c$, one sees that the Reynolds stress is smaller than the surface drag, because there is a small erosion of the upward waves in the inner layer. Interestingly, there is a marked difference between the neutral and stratified cases near the cut-off wavenumber with the trapped mode appearing near the cut-off wave number as a narrow peak in the surface drag (see Fig. 4c). The cases with more evanescent modes in Figs. 4b and 4d, are dynamically much richer. In them, one sees that in the propagating harmonics range ($k < k_c$) drag and wave Reynolds stress almost coincide, whereas in the evanescent harmonics range ($k > k_c$) the drag can be large, whereas the Reynolds stress is almost zero. More specifically, the large drag when $F = 4$ and $J = 0.1$ in Fig. 4b is not likely due to trapped waves, as the signal on vertical velocity downstream of the mountain in Fig. 3b is very small. It is a case where evanescent harmonics essentially contribute via a turbulent orographic form drag. On the contrary, when $J = 1$ and still for $F = 4$, Fig. 4d shows a substantial peak in drag at $k \approx 0.4$, which corresponds to the horizontal wavelength that dominates the response in Fig. 3d.

3.3 | Mountain drag and gravity wave stress predictors

Based on the fact that the vertical velocity field scales in amplitude as if the background flow incident on the mountain should be taken at the inner altitude, we propose as a first predictor of the wave drag its hydrostatic value:

$$\widehat{D}_W(k) = \rho_r C_W \, k \, \widehat{h}\widehat{h}^* \, U(h_i(k)) \, N(h_i(k)), \tag{16}$$

where the constant C_W is a tunable parameter. The physical interpretation is that the strong turbulent diffusion in the lower part of inner layer forces the streamlines to follow the hills, and the distorted streamlines become the "effective" orography that produces the waves (see Lott et al., 2020). We also consider that turbulent form drag is the result of the pressure loss across the hill that balances changes in disturbance shear stress. To estimate it we consider that

the amplitude of the horizontal wind disturbance at h_i is $\approx \widehat{h}\partial U/\partial Z(h_i)$, an estimate based on the particular solution of the problem in curved coordinates, (see (A24) in Lott et al., 2023). Taking into account the definition of $h_i(k)$ in (14) and comparing the horizontal pressure gradient to the shear stress vertical derivative (see right hand side in (31)) yields $ik\widehat{p}^* \approx U(h_i)\partial U/\partial Z(h_i)\widehat{h}$. Multipliying by $\widehat{h}^*$ gives an estimate of the turbulent form drag,

$$\widehat{D}_T(k) = \rho_r C_T\, k\, \widehat{h}\widehat{h}^*\, U(h_i(k))\, \frac{\partial U(h_i(k))}{\partial Z}, \tag{17}$$

C_T being a second tunable parameter. This is an interesting formula since compared to (16), the Brunt-Vaisala frequency, $N(h_i)$ is simply replaced by the wind shear $\partial U/\partial Z(h_i)$.

The dashed red curve in Fig. 4 applies the gravity wave stress predictor for harmonics with $k < k_c$ and taking $C_W = 0.4$. We see that it matches well the gravity wave stress from the model for all values of F and J. For the surface pressure drag we augment gravity wave predictor (16) with turbulent form drag predictor (17) taking $C_T = 0.1$, resulting in surface drag

$$\widehat{D}_S(k) = \widehat{D}_T(k) + \Theta(k_c - k)\,\widehat{D}_w(k), \tag{18}$$

with Θ for the Heaviside function to retain propagating modes for $k < k_c$ only. For small Froude number, the black dashed lines shows that the inclusion of the turbulent form drag does not change much the prediction. It slightly increases the drag compared to the gravity wave stress predictor, staying quite close to the model drag. Of course none of these two formulae capture the peaks in drag near k_c (Fig. 4c). At large Froude number, the results are more contrasted between the neutral and stratified case. In both, our predictors stay valid for propagating disturbances ($k < k_c$) and the drag predictor seems to work quite well as long as there are no trapped waves, which is valid in the neutral case (see Fig. 4b). However, the predictor rather fails in the stable case, when trapped waves control the flow at low level (see Fig. 4d). Unfortunately, there is no simple way to capture the drag due to quasi-resonant dissipative modes. The only analytical results we have, stay limited to an inviscid and simplified background configurations (Teixeira et al., 2013a,b). To circumvent that difficulty we return to the fact that when the turning levels are sufficiently high, the hydrostatic wave theory is still suitable for the prediction of drag (Lott, 1998) but overstate it when the turning levels are close to the surface. These are inviscid results, but here we have seen that trapped lee waves do not develop when $k < 1/h_t(k)$ and become strong when $k > 1/h_t(k)$. For this reason, we next propose to extend the wave drag predictor to the evanescent modes satisfying this criteria and write,

$$\widehat{D}_S(k) = \mathbf{D}_T(k) + \Theta(kh_t(k) - S_t)\,\mathbf{D}_w(k), \tag{19}$$

where S_t is a tunable parameter. Note that all the propagating harmonics are included in (19) since $h_t(k) = \infty$ when $k < k_c$. In Fig. 4d, we take $S_t = 1$ and see on the green dotted curve that this extension of the gravity wave drag to the evanescent sector permits to capture a fraction of the peak in drag that is due to trapped waves. In the other panels, this extension does not play a role simply because the h_t's are too close to the surface when not infinite. We have tested our formula with many different flow configurations, varying λ, z_o, J and F quite systematically. When we change λ and z_o for instance, we found quite comparable behaviour as in Lott et al. (2023), namely that predictors comparable to ours here stay qualitatively valid. It means that matches can be obtained for slightly different tuning parameters C_W and C_T. What is important here are the concepts. But to illustrate the difficulties, Fig. 4a-b shows

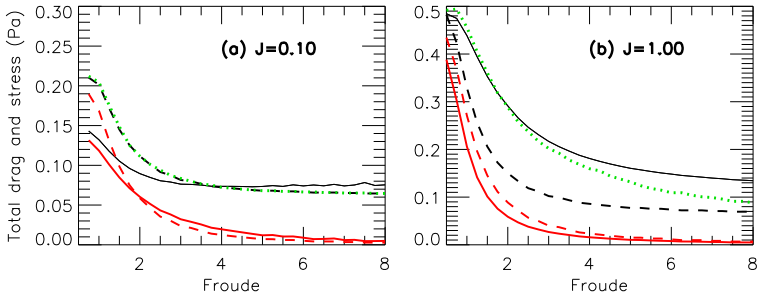

FIGURE 5 Drag integrated over wave number for the Gaussian hill, as a function of the Froude number with J=0.1 (left panel) and J=1 (right panel). The solid black curve is for surface drag and the solid red curve for gravity wave stress both from the linear model. The dashed black curve represents the TOFD predictor, the dashed red the gravity wave stress predictor, and the dotted green curve includes TOFD + gravity wave + trapped waves predictors according to eq. (19).

the drag stresses and predictors integrated over all wavenumbers,

$$D(Z) = 2\pi \int_{-\infty}^{+\infty} \mathbf{D}(k, Z)\, dk \tag{20}$$

and varying systematically the Froude number. In them one sees that it is the wave stress that is the most accurately predicted with some overestimation in the neutral case at small Froude number. This impacts the surface drag predictor in the same range. At Froude number $F > 1$, the wave stress is well predicted in both neutral and stratified cases. The difference between the surface drag and the gravity wave stress is important because it tells us where an additional tendency is needed in the momentum equation. It is particularly important important at large Froude number in both the neutral and stratified case. In the neutral case, the TOFD predictor captures well the difference as indicated by the dashed line in Fig. 5a. In the stratified case, the TOFD predictor increases the wave drag, but not sufficiently, it is the inclusion of trapped waves that make up the difference (see the green dotted line in Fig. 5b). Clearly at large Froude number the predictor starts to diverge from the model, underestimating the trapped waves contribution. We found such underestimations quite common but better predictors of the trapped waves are hard to find.

As our linear dissipative theory attributes the differences between surface drag and wave stress to three different causes, inner layer erosion of propagating modes, inner layer erosion of evanescent modes, or dissipated trapped lee waves, we can ask ourselves if the drag at low level will be distributed differently in the vertical. For this purpose, Fig. 6 shows vertical profiles of the MFs $\mathbf{D}(k, Z)$ for different wave numbers, where for each wavenumber the altitudes has been normalized by the inner layer altitude. When there are almost no evanescent modes in the neutral case (Fig. 6a), the MFs are almost uniform although some erosion occurs below $z < 3\, to\, 4h_i(k)$ in the stable case (Fig. 6b). Compared to Fig. 6a there is some erosion of the MFs because the gravity waves have a shorter vertical wavelength and are hence more affected by dissipation (see Pauget et al., 2024). At large Froude numbers, most of the evanescent harmonics that contribute to the drag see their MFs decreasing between the surface and $z < 3$ to $, 4h_i(k)$ again. This is the same vertical distance over which the propagating harmonics are affected. Whatever the dynamics, from the many dissipated evanescent harmonics seen in $Fig.\ 6b$, to the trapped mode that strongly contributes in Fig. 6d, the MFs always decrease over the same distance, which is about $3\, to\, 4h_i(k)$. Of course this is not a surprise, all modes being steady we know from Eliassen and Palm (1962) that the MFs can only decay where there is dissipation, which here

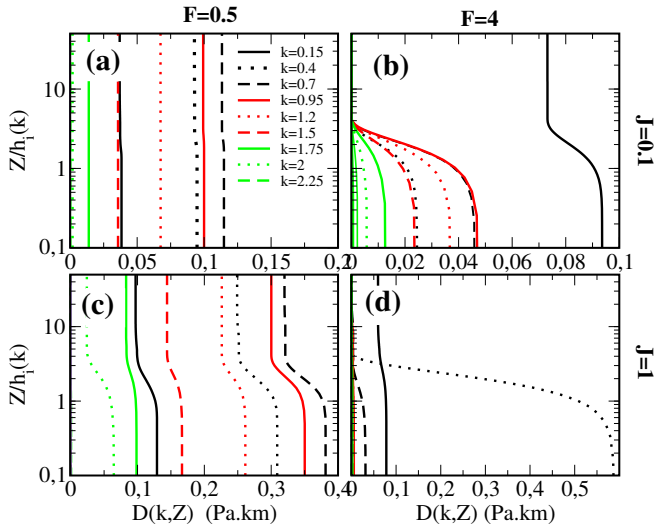

FIGURE 6 Vertical profiles of momentum fluxes $\widehat{D}(k, Z)$ for a range of wave numbers (see legend, with k in km^{-1}).

occurs over distances scaled by h_i.

3.4 | Predicting blocking/sheltering depth

The fundamental concept used to predict flow blocking in Lott and Miller (1997) is that according to Smith (1980), linear theory can be used to predict the blocking altitude. More specifically, in Lott and Miller (1997) it tells at which altitude an air parcel, initially located at an altitude z_b, and forced to move up, will no longer ascent vertically when reaching the mountain top. Basically, and using a WKB approach, we therefore have to calculate the change in phase between z_b and the mountain top H and test when it exceeds a threshold H_{NC}

$$\int_{z_b}^{H} \frac{N}{U} dz = H_{NC}. \tag{21}$$

Here we have used the hydrostatic approximation to express a local vertical wavenumber. We could alternatively get closer to the Smith (1980)'s approach and search when the horizontal velocity produced by the wave forced by a hill of height $H - z_b$ balances the incident wind at that height. Still in the hydrostatic case this gives

$$N(z_b)\,(H - z_b) \approx U(z_b) * H_{NC}. \tag{22}$$

It is not the same, but quite comparable. Advantage of (22) is that it can easily be extended to the non-hydrostatic case. If we use linear WKB theory to calculate u' produced by $h(x) - z_b$ it writes,

$$u' = U(z_b) \int_{-\infty}^{+\infty} -i\,\mathrm{sign}(k) \sqrt{\frac{N^2}{U^2} - k^2}\,(\mathbf{h} - \mathbf{z_b}) dk. \tag{23}$$

We can simplify further and consider that the Fourier transform of the hill above the blocked flow stays near the Fourier transform of the hill, $\widehat{h} - \widehat{z}_b = (H - z_b)\ \widehat{h}/H$, in which case, the condition $|u'| \approx H_{NC} U$ writes:

$$\frac{H - z_b}{H} \int_{-\infty}^{+\infty} \sqrt{\left| \frac{N(z_b)^2}{U(z_b)^2} - k^2 \right|} \widehat{h}(k)\, dk \approx H_{NC}. \tag{24}$$

In case of uniform flow and Gaussian ridge, $\mathbf{h} = \frac{LH}{\sqrt{2\pi}} e^{\frac{-k^2 L^2}{2}}$ this condition reduces to

$$\frac{(H - z_b) N(z_b)}{U(z_b)} = H_{NC}, \text{ and } \frac{2}{\sqrt{\pi}} \frac{(H - z_b)}{L} = H_{NC}. \tag{25}$$

in the hydrostatic stratified case and in the non-hydrostatic neutral case respectively. We recognize the criteria for the non-dimensional height used in stratified flow dynamics and a slope criterion in the neutral case.

4 | SUMMARY AND DISCUSSION

4.1 | Upgrading TOFD and SSO

The assumption of most parameterizations of subgrid scale mountains is that mountain flow dynamics can be described by three conceptual models whose relevance depends on a non-dimensional mountain height, $H_N = HN/|U|$ and slope $S = H/L$ parameters.

For small H_N and very small slope S, the mountain drag is due to "upward" propagating waves, whose value is estimated via hydrostatic predictors. In our Boussinesq 2D framework this drag due to Upward propagating Waves (UW) can be written as

$$D_{UW} = \overline{U}\,\overline{N} \int_0^{\infty} \rho_r C_w k \widehat{h}\widehat{h}^* dk, \tag{26}$$

where $\overline{U}$ and $\overline{N}$ are typically averaged between the surface (or a blocked flow altitude) and the mountain top. The fact that the incident winds and stability estimate are independent of wavenumber eases integration, and this assumption is made in all existing schemes, to our knowledge. In our calculation, we propose to change this into

$$D_{UW} = \int_0^{k_c} C_w \rho_r k \widehat{h}\widehat{h}^* U(h_i) N(h_i) dk, \tag{27}$$

which is quite close, at least conceptually. We take into account non-hydrostatic effects by limiting the contribution of the upward propagating waves to those not reaching turning levels in the lower troposphere, which requires to identify k_c. The momentum deposit due to those waves can be treated using conventional breaking criteria. A difficulty in our case, is that the level at which U and N are evaluated varies with wavenumber which complexifies the integration. In terms of amplitude nevertheless, the fact that we propose to take winds and stability at inner layer altitude should not make a big difference because boundary layer turbulence smears out disturbances typically over a depth of more than 100m. At the current resolution of most models, these altitudes should not be too far from those of the subgrid scale orography. Treating breaking could either be done harmonic by harmonic, or by making hypotheses on the spectral distribution of the wave induced vertical displacement to detect overturning and limit it.

Still at small H_N but larger S, when the incident flow is more neutral, TOFD drag needs to be applied. Following

eq (9) in Beljaars et al. (2004) it writes

$$D_T = \int_{k_0}^{\infty} \rho_r C_T k^2 \widehat{hh^*} \, |U(h_m)|^2 \, dk, \text{ where the height } h_m = c_m/k \tag{28}$$

where C_T and c_m are tunable parameters. This expression translates linear dynamics (the drag is proportional to the square of the slope) and we propose to modify it into,

$$D_T = \int_{0}^{\infty} \rho_r C_T k \widehat{hh^*} \, |U(h_i)| \left| \frac{dU}{dZ}(h_i) \right| dk. \tag{29}$$

In our framework, the inner layer height is the height at which background turbulence affects disturbances, and can be quite high, e.g. around 100 m for our 1km long ridges (see Fig. 2) whereas Beljaars et al. (2004) take $c_m = 0.1$ which results in comparable altitudes. Concerning the vertical distribution of the drag, it is done for each harmonic over scale $l_w = 2/k$ capped by around 500 m in Beljaars et al. (2004) , again comparable to the decay over $3h_i - 4h_i$ seen here in Fig. 6. Note that Beljaars et al. (2004) then make other simplifications and integrate over wavenumber to fasten the parameterization and ensure its stability, which we leave for further analysis. A novelty here is that we propose to include a trapped wave drag at low level, acting on the same depth as D_T, and which is just the wave drag extended between k_c and k_t:

$$D_{TW} = \int_{k_c}^{k_t} C_w \rho_r k \widehat{hh^*} U(h_i) N(h_i) dk., \text{where } k_t h_t(k_t) = S_T \tag{30}$$

and where S_t is another tuning parameter ($S_t = 1$ in our calculations, see (Figs. 4-5)). The extension of the wave drag at trapped wavenumbers here could provide the low level drag needed in the stable case when the turbulent drag is not strong enough (the long-tail problem see Tsiringakis et al. (2017)). There is a marked difference nevertheless: the wave drag in Tsiringakis et al. (2017) is evaluated with wind and stratification taken at the boundary layer height, and is entirely redistributed over that height. There is no distinction between trapped or freely propagating waves, and the dynamics at work is more related to freely propagating waves reaching critical levels in the boundary layer (Nappo and Chimonas, 1992). In our case, the low level drag is explicitly due to trapped waves. Critical levels can also occur but only for the upward waves contributing to the drag in (27) providing that we treat their propagation and breaking according to the direction of their horizontal wavenumber (Martin and Lott, 2007).

Finally, for large H_N and/or S we kwow that part of the flow is either blocked upstream (large H_N, small S) or downstream (the sheltering effect occurring in the neutral case (large S, small H_N). Without checking numerically, we propose to replace conventional blocked flow criteria like in (21) by its non-hydrostatic extension (24). Next step could be to apply low level drag below that level, as it is described in Lott and Miller (1997) (see Eqs. 4 and 5).

4.2 | Discussion and further challenges

As weather prediction and climate model resolution increases and gravity waves at least become partly resolved, it could mean that a tipping point will soon be reached in the domain of subgrid scale orography parameterization. It may well be that gravity waves and related nonlinear processes (flow blocking) no longer need to be parameterized and that we should only consider how the unresolved subgrid scale orography feeds turbulence. For a variety of reasons, which include that the model gridscale is not representative of the model effective resolution, it does not seem to be the case in the foreseen future. Nevertheless, it is quite certain that models are reaching scales where the

interplay between gravity waves and turbulent boundary layers should be considered. The example we provide here of a simplified boundary layer interacting with a small slope hill, is a first step in this direction. By proposing moderate changes in existing parameterizations, it illustrates how they can be combined. For example, the often assumed scale separation between TOFD and SSO parameterization needs to be made flow dependent, and we show here that it could be done by evaluating a cut-off wave number k_c obtained for instance by minimizing the Scorer parameter in the troposphere. We also show that wave drag and turbulent orographic form drag could have similar expressions, simply changing the buoyancy frequency N into wind shear $\partial U/\partial Z$ when neutral dynamics start to dominate. Also, trapped lee waves can be taken into account by comparing the horizontal wavenumber of each harmonic to their turning height altitude.

Beyond this quite reasonable results, and even giving credit to the predictors we provide, numerous difficulties remain. First, our drag expressions need to be integrated over wavenumbers, which is potentially involved and may necessitate numerous idealized tests using single column models and realistic orographic spectra (Beljaars et al., 2004). There is also the difficulty of accounting for turning levels, for instance when the wind turns with altitude within the boundary layer (Shutts, 1995; Martin and Lott, 2007). Also, all our background fields and predictors involve inner layer depths, which measure the altitude at which turbulence impacts subgrid scale dynamics, and that can be difficult to evaluate. If it can not be worked out from the boundary layer scheme where a disturbance dissipates, other solutions may exist like taking the inverse of the horizontal wavenumber as in Beljaars et al. (2004), or a mid-level altitude as in Hunt et al. (1988b) but these need further study.

Although we think that this study offers improvements over existing schemes for subgrid orogaphy, we also recognise the limitations that need further work. The simplest improvement is probably the extension to 3D orography particularly if it is assumed that subgrid orography is isotropic. Impact studies have shown that the impact of anisotropy is very limited (Elvidge et al., 2019). In the current study, the turbulence model is a mixing length scheme, but it does not consider the influence of stability on turbulent diffusion. It does also not consider non-equilibrium aspects. As most turbulence schemes in large scale meteorological models, "quasi-equilibrium" is assumed i.e changes in the forcing are assumed to be slow compared to the time scale that turbulence needs to establish equilibrium. The latter is a good approximation particularly close to the surface where the turbulence time scales are short, but it becomes less accurate for perturbations from subgrid orography. For those cases Beljaars et al. (1987) have shown that higher order closure is important particularly to simulate stress profiles. In a review of schemes, Xu and Taylor (1995) conclude that the level of closure is more important for the simulation of surface drag than using a full non-linear model.

More fundamentally, if our calculations somehow take into account the impact of turbulence on waves and on the wave duct, they completely neglect the feedback of waves on the turbulence itself, and additional mixing may occur (Sun et al., 2015; Vosper et al., 2018). Our calculations also neglect that enhanced subgrid scale mixing is more likely to occur on the lee side of the mountains, for instance where trapped waves produce rotors. In this case, the trapped waves can produce vertical exchange of heat, a possibility we have completely excluded here.

5 | DATA AVAILABILITY STATEMENT

The theoretical model used to support the findings of this study is available from the corresponding author upon request.

Appendix

Recalling from (3) that the vertical coordinate transform writes $z = Z + f(Z)h(x)$ and neglecting turbulent diffusion terms in the horizontal (Prandtl approximation), the linear set as solved in Lott et al. (2023) can be rewritten in the dimensional form,

$$ikU\widehat{u} + \frac{\partial U}{\partial Z}\widehat{\mathbf{w}} + ik\frac{\widehat{p}}{\rho_r} = \frac{\partial}{\partial Z}\Big\{\underbrace{2lu_*}_{incl\ \nu'}\frac{\partial \widehat{u}}{\partial Z}\Big\} + ikBf\widehat{h} \tag{31a}$$

$$ikU\widehat{b} + \frac{\partial B}{\partial Z}\widehat{\mathbf{w}} = \frac{\partial}{\partial Z}\Big\{lu_*\frac{\partial \widehat{b}}{\partial Z} + lb_*\frac{\partial \widehat{u}}{\partial Z}\Big\}, \tag{31b}$$

$$ikU\widehat{\mathbf{w}} + \frac{1}{\rho_r}\frac{\partial \widehat{p}}{\partial Z} - \widehat{b} = k^2U^2f\widehat{h}, \tag{31c}$$

$$ik\widehat{u} + \frac{\partial \widehat{\mathbf{w}}}{\partial Z} = -ikU\frac{df}{dZ}\widehat{h}, \tag{31d}$$

$$\text{where } \widehat{\mathbf{w}} = \widehat{w} - ikUf\widehat{h}, \tag{31e}$$

subject to the surface boundary condition ($\widehat{u} = \widehat{\mathbf{w}} = \widehat{b} = 0$ in $Z = 0$). In curved coordinates the mountain forcing is applied via the last terms on the right of (31a), (31c), and (31d).

references

Ayotte, K. (2008) Computational modelling for wind energy assessment. *Journal of Wind Engineering and Industrial Aerodynamics*, 1571–1590.

Belcher, S. and Hunt, J. (1998) Turbulent flow over hills and waves. *Annual Review of Fluid Mechanics*, **30**, 507–538.

Belcher, S. E. and Wood, N. (1996) Form and wave drag due to stably stratified turbulent flow over low ridges. *Quart. J. Roy. Meteor. Soc.*, **122**, 863–902.

Beljaars, A., Walmsley, J. and Taylor, P. (1987) A mixed spectral finite-difference model for neutrally stratified boundary-layer flow over roughness changes and topography. *Boundary-Layer Meteorology*, **38**, 273–303.

Beljaars, A. C. M., Brown, A. R. and Wood, N. (2004) A new parametrization of turbulent orographic form drag. *Quarterly Journal of the Royal Meteorological Society*, **130**, 1327–1347.

Blackadar, A. K. (1962) The vertical distribution of wind and turbulent exchange in a neutral atmosphere. *Journal of Geophysical Research*, **67**, 3095–3102.

Charru, F., Andreotti, B. and Claudin, P. (2012) Sand ripples and dunes. *Annu. Rev. Fluid Mech.*, **45**, 469–493.

Clark, T. L. (1977) A small-scale dynamic model using a terrain-following coordinate transformation. *Journal of Computational Physics*, **24**, 186–215.

Durran, D. R. (1990) Mountain waves and downslope winds. *AMS Meteorological Monographs*, **23**, 59–83.

Eliassen, A. and Palm, E. (1962) On the transfer of energy in stationnary mountain waves. *Geophys. Publ.*, **22**, 1–23.

Elvidge, A. D., Sandu, I., Wedi, N., Vosper, S. B., Zadra, A., Boussetta, S., Bouyssel, F., van Niekerk, A., Tolstykh, M. A. and Ujiie, M. (2019) Uncertainty in the representation of orography in weather and climate models and implications for parameterized drag. *Journal of Advances in Modeling Earth Systems*, **11**, 2567–2585.

Giorgetta, M. A., Brokopf, R., Crueger, T., Esch, M., Fiedler, S., Helmert, J., Hohenegger, C., Kornblueh, L., Köhler, M., Manzini, E., Mauritsen, T., Nam, C., Raddatz, T., Rast, S., Reinert, D., Sakradzija, M., Schmidt, H., Schneck, R., Schnur, R., Silvers, L., Wan, H., Zängl, G. and Stevens, B. (2018) Icon-a, the atmosphere component of the icon earth system model: I. model description. *Journal of Advances in Modeling Earth Systems*, **10**, 1613–1637.

Hunt, J. C. R., Leibovich, S. and Richards, K. J. (1988a) Turbulent shear flows over low hills. *Quart. J. Roy. Meteor. Soc.*, **114**, 1435–1470.

Hunt, J. C. R., Richards, K. J. and Brighton, P. W. M. (1988b) Stably stratified shear flow over low hills. *Quart. J. Roy. Meteor. Soc.*, **114**, 859–886.

Hájková, D. and Šácha, P. (2024) Parameterized orographic gravity wave drag and dynamical effects in cmip6 models. *Climate Dynamics*, 2259–2284.

Jackson, P. S. and Hunt, J. C. R. (1975) Turbulent wind flow over low hill. *Quart. J. Roy. Meteor. Soc.*, **101**, 929–955.

Kim, Y.-j. and Doyle, J. D. (2005) Extension of an orographic-drag parametrization scheme to incorporate orographic anisotropy and flow blocking. *Quarterly Journal of the Royal Meteorological Society*, **131**, 1893–1921.

Lindzen, R. S. (1981) Turbulence and stress owing to gravity wave and tidal breakdown. *Journal of Geophysical Research: Oceans*, **86**, 9707–9714.

Lott, F. (1998) Linear mountain drag and averaged pseudo-momentum flux profiles in the presence of trapped lee waves. *Tellus A: Dynamic Meteorology and Oceanography*.

Lott, F., Beljaars, A., Pauget, L., Deremble, B. and Millet, C. (2023) Neutral and stratified turbulent boundary layer flow over low mountains. *Quart. J. Roy. Meteor. Soc.,202*, **Submitted**.

Lott, F., Deremble, B. and Soufflet, C. (2020) Mountain waves produced by a stratified shear flow with a boundary layer. part ii: Form drag, wave drag, and transition from downstream sheltering to upstream blocking. *Journal of the Atmospheric Sciences*.

Lott, F. and Miller, M. (1997) A new subgrid scale orographic drag parameterization; its testing in the ecmwf model. *Quart. J. Roy. Meteor. Soc.*, **123**, 101–127.

Martin, A. and Lott, F. (2007) Synoptic responses to mountain gravity waves encountering directional critical levels. *Journal of the Atmospheric Sciences*, **64**, 828 – 848. URL: `https://journals.ametsoc.org/view/journals/atsc/64/3/jas3873.1.xml`.

McFarlane, N. (1987) The effect of orographically excited gravity wave drag on the general circulation of the lower stratosphere and troposphere. *Journal of Atmospheric Sciences*, **44**, 1775–1800.

Nappo, C. J. and Chimonas, G. (1992) Wave exchange between the ground surface and a boundary-layer critical level. *Journal of Atmospheric Sciences*, **49**, 1075 – 1091. URL: `https://journals.ametsoc.org/view/journals/atsc/49/13/1520-0469_1992_049_1075_webtgs_2_0_co_2.xml`.

van Niekerk, A. and Vosper, S. (2021) Towards a more "scale-aware" orographic gravity wave drag parametrization: Description and initial testing. *Quarterly Journal of the Royal Meteorological Society*, **147**, 3243–3262.

Palmer, T. N., Shutts, G. J. and Swinbank, R. (1986) Alleviation of systematic westerly bias in general circulation and numerical weather prediction models through an orographic gravity wave drag parametrization. *Quart. J. Roy. Meteor. Soc.*, **112**, 2056–2066.

Pauget, L., Lott, F. and Millet, C. (2024) Mountain waves developing inside and aloft stably stratified turbulent boundary layers. *Quarterly Journal of the Royal Meteorological Society*, **150**, 4594–4608.

Pithan, F., Shepherd, T. G., Zappa, G. and Sandu, I. (2016) Missing orographic drag leads to climate model biases in jet streams, blocking and storm tracks. *Geophysical Research Letters*, **43**, 7231–7240.

Sandu, I., Bechtold, P., Beljaars, A., Bozzo, A., Pithan, F., Shepherd, T. and Zadra, A. (2015) Impacts of parameterized orographic drag on the northern hemisphere winter circulation, journal of advances in modeling earth systems. *J. Adv. Model. Earth Syst.*, **8**, 196–211.

Schär, C. and Durran, D. R. (1997) Vortex formation and vortex shedding in continuously stratified flows past isolated topography. *Journal of the Atmospheric Sciences*, **54**, 534 – 554.

Schär, C. and Smith, R. B. (1993) Shallow-water flow past isolated topography. part i: Vorticity production and wake formation. *Journal of Atmospheric Sciences*, **50**, 1373 – 1400.

Scinocca, J. F. and McFarlane, N. A. (2000) The parametrization of drag induced by stratified flow over anisotropic orography. *Quarterly Journal of the Royal Meteorological Society*, **126**, 2353–2393.

Shutts, G. (1995) Gravity-wave drag parametrization over complex terrain: The effect of critical-level absorption in directional wind-shear. *Quarterly Journal of the Royal Meteorological Society*, **121**, 1005–1021.

Smith, R. B. (1980) Linear theory of stratified hydrostatic flow past an isolated mountain. *Tellus*, **32**, 348–364.

Sun, J., Nappo, C. J., Mahrt, L., Belušić, D., Grisogono, B., Stauffer, D. R., Pulido, M., Staquet, C., Jiang, Q., Pouquet, A., Yagüe, C., Galperin, B., Smith, R. B., Finnigan, J. J., Mayor, S. D., Svensson, G., Grachev, A. A. and Neff, W. D. (2015) Review of wave-turbulence interactions in the stable atmospheric boundary layer. *Reviews of Geophysics*, **53**, 956–993.

Teixeira, M., Argaín, J. and Miranda, P. (2013a) Drag produced by trapped lee waves and propagating mountain waves in a two-layer atmosphere. *Quarterly Journal of the Royal Meteorological Society*, **139**, 964–981.

— (2013b) Drag produced by trapped lee waves and propagating mountain waves in a two-layer atmosphere. *Quarterly Journal of the Royal Meteorological Society*, **139**, 964–981. URL: `https://rmets.onlinelibrary.wiley.com/doi/abs/10.1002/qj.2008`.

Tsiringakis, A., Steeneveld, G. J. and Holtslag, A. A. M. (2017) Small-scale orographic gravity wave drag in stable boundary layers and its impact on synoptic systems and near-surface meteorology. *Quarterly Journal of the Royal Meteorological Society*, **143**, 1504–1516.

Vosper, S. B. (2015) Mountain waves and wakes generated by south georgia: implications for drag parametrization. *Quarterly Journal of the Royal Meteorological Society*, **141**, 2813–2827.

Vosper, S. B., Brown, A. R. and Webster, S. (2016) Orographic drag on islands in the nwp mountain grey zone. *Quarterly Journal of the Royal Meteorological Society*, **142**, 3128–3137.

Vosper, S. B., Ross, A. N., Renfrew, I. A., Sheridan, P., Elvidge, A. D. and Grubišić, V. (2018) Current challenges in orographic flow dynamics: Turbulent exchange due to low-level gravity-wave processes. *Atmosphere*, **9**.

Weng, W., Chan, L., Taylor, P. and Xu, D. (1997) Modelling stably stratified boundary-layer flow over low hills. *Quarterly Journal of the Royal Meteorological Society*, **123**, 1841–1866.

Wood, N., Brown, A. and Hewer, F. (2001) Parameterizing the effects of orography on the boundary layer: an alternative to effective roughness lengths. *Quart. J. Roy. Meteor. Soc.*, **127**, 759–777.

473 Wood, N. and Mason, P. (1993) The pressure force induced by neutral, turbulent flow over hills. *Quart. J. Roy. Meteor. Soc.*,
474 **119**, 1233–1267.

475 Xu, D. and Taylor, P. A. (1995) Boundary-layer parametrization of drag over small-scale topography. *Quarterly Journal of the*
476 *Royal Meteorological Society*, **121**, 433–443.

Long Solution in curved coordinates

U =cte, $N^2 = \frac{\partial B}{\partial z}$=cte, no friction $f(Z) = 1$:

$$ikU\widehat{u} + ik\frac{\widehat{p}}{\rho_r} = ikB\widehat{h} \tag{32a}$$

$$ikU\widehat{b} + \frac{\partial B}{\partial Z}\widehat{\mathbf{w}} = 0, \tag{32b}$$

$$ikU\widehat{\mathbf{w}} + \frac{1}{\rho_r}\frac{\partial \widehat{p}}{\partial Z} - \widehat{b} = k^2U^2\widehat{h}, \tag{32c}$$

$$ik\widehat{u} + \frac{\partial \widehat{\mathbf{w}}}{\partial Z} = 0, \tag{32d}$$

$$\text{where } \widehat{\mathbf{w}} = \widehat{w} - ikU\widehat{h}, \tag{32e}$$

Particular solution:

$$\hat{p}_p = P_z\hat{h} = \rho_r B\hat{h},\ \hat{b}_p = B_z\hat{h} = N^2\hat{h},\ \widehat{\mathbf{w}}_p = -ikU\hat{h},\ \hat{u}_p = 0. \tag{33}$$

Homogeneous solution:

$$\frac{d^2\widehat{\mathbf{w}}_h}{dZ^2} + \left(\frac{N^2}{U^2} - k^2\right)\widehat{\mathbf{w}}_h = 0 \rightarrow \widehat{\mathbf{w}}_h = \widehat{\mathbf{w}}_h(0)e^{imZ} \tag{34}$$

Boundary condition:

$$\left(\widehat{\mathbf{w}}_p + \widehat{\mathbf{w}}_h\right)(Z = 0) = 0 \rightarrow \widehat{\mathbf{w}}_h(0) = ikU\hat{h} \tag{35}$$

Complete solution:

$$\widehat{\mathbf{w}} = ikU\hat{h}e^{imz} - ikUh,\ \hat{u} = imU\hat{h}e^{imz},\ \frac{\hat{p}}{\rho_r} = B\hat{h} - imU^2\hat{h}e^{imz} \tag{36}$$

Drag according to (15):

$$-\rho_r\left(mkU^2\hat{h}\hat{h}^* - kmU^2\hat{h}\hat{h}^*e^{imz}\right) + ik\rho_r B\hat{h}\hat{h}^* - mk\rho_r\hat{h}\hat{h}^*U^2e^{-imz} \tag{37}$$

Imaginary part only keep first term. A lot of cancelation compared to rectangular coordinates.